Journal of Physics D: Applied Physics

PAPER

Numerical simulation of the flow characteristics inside a novel plasma spray torch

To cite this article: Sen-Hui Liu *et al* 2019 *J. Phys. D: Appl. Phys.* **52** 335203

IOP Publishing Journal of Physics D: Applied Physics

J. Phys. D: Appl. Phys. **52** (2019) 335203 (17pp) https://doi.org/10.1088/1361-6463/ab228b

Numerical simulation of the flow characteristics inside a novel plasma spray torch

Sen-Hui Liu[1,2], Juan Pablo Trelles[2], Anthony B Murphy[3], Lu Li[4], Shan-Lin Zhang[1], Guan-Jun Yang[1], Cheng-Xin Li[1,5] and Chang-Jiu Li[1]

[1] State Key Laboratory for Mechanical Behavior of Materials, School of Materials Science and Engineering, Xi'an Jiaotong University, Xi'an, Shaanxi 710049, People's Republic of China
[2] Department of Mechanical Engineering, University of Massachusetts, Lowell, MA 01854, United States of America
[3] CSIRO Manufacturing, Lindfield, NSW 2070, Australia
[4] Zhenhuo Plasma Technology Company, Chengdu, Si Chuan 610065, People's Republic of China

E-mail: licx@mail.xjtu.edu.cn

Received 14 December 2018, revised 1 May 2019
Accepted for publication 17 May 2019
Published 18 June 2019

Abstract

A novel direct current non-transferred arc plasma torch that can generate a long, stable and silent plasma jet of over 350 mm in length into ambient air is studied by numerical modelling. Numerical simulation of the plasma torch operating in the current of 160 A with a mixture of 70% nitrogen and 30% argon in volume at three different gas flow rates (8.5 SLPM, 10 SLPM and 14 SLPM) are performed in a 3D domain. The renormalization group method is employed to model the turbulent flow inside the plasma torch, particularly the torch's novel channel structure. The results show that a narrow circular gap at the boundary layer of the cathode led to a region of high flow constriction and large pressure and velocity gradients. The anode counts with a novel trumpet-like structure that separates the flow in the channel and induces turbulent fluctuations in the direction transverse to the flow, which can disrupt and decrease the cold boundary layer around the arc column. The arc attachment position that obtained in simulation is in agreement with the experiment observation. The maximum velocity at the torch nozzle in simulation is increased and the length of the plasma jet in experiment is decreased with the increasing of the total gas flow rates from 8.5 SLPM, 10 SLPM to 14 SLPM. However, the maximum temperature at the torch nozzle in three different gas flow rates are varied slightly. Our results suggest that generation of a long and stable plasma jet downstream of the nozzle exit should not only focus on a relatively low gas flow rate, but depend instead on the aerodynamic characteristics of the channel flow, particularly in the anode region and downstream of the anode.

Keywords: plasma spraying, numerical simulation, 3D flow, rng model

(Some figures may appear in colour only in the online journal)

[5] Author to whom any correspondence should be addressed.

Notation

$\boldsymbol{A}$	Magnetic vector potential (T m^{-1})
$\boldsymbol{B}$	Magnetic field (T)
C_p	Specific heat at constant pressure (J (kg K)$^{-1}$)
$\boldsymbol{E}$	Electric field (V m^{-1})
E	Elementary charge (1.602×10^{-19} C)
F_r, F_θ, F_z	Components of Lorentz force in r, θ and z direction
$\boldsymbol{F}$	Lorentz force (N m^{-3})
W	Power (W)
I	Current (A)
I'	Turbulent intensity (%)
K	Turbulent kinetic energy (m^2 s^{-2})
k_B	Stefan–Boltzmann constant (5.67×10^{-8} W (m^2 K^4)$^{-1}$)
P	Pressure (Pa)
Q	Gas flow rate (kg s^{-1})
R_c	Radius of curvature of the anode column (m)
T	Gas temperature (K)
J_{cath}	Current density at cathode tip (A m^{-2})
j_r, j_θ, j_z	Components of current density in r, θ and z direction (A m^{-2}).
$\boldsymbol{J}$	Current density (A m^{-2})

Greek symbols

ε_r	Net emission coefficient (W (m^3 sr)$^{-1}$)
κ	Thermal conductivity (W (m K)$^{-1}$)
μ	Dynamic viscosity (kg (m s)$^{-1}$)
μ_t	Turbulent viscosity (kg (m s)$^{-1}$)
μ_{eff}	Effective viscosity (kg (m s)$^{-1}$)
σ	Electrical conductivity (S m^{-1})
ρ	Density (kg m^{-3})
ϕ	Electric potential (V)

Abbreviations

LES	Large eddy simulation
LTE	Local thermodynamic equilibrium.
RANS	Reynolds-averaged Navier–Stokes
RNG	Renormalization group method
MHD	Magnetohydrodynamic
NEC	Net emission coefficient

1. Introduction

In direct current (dc) non-transferred arc plasma torches, an electric arc is formed across a cylindrical channel between an upstream conical cathode and a downstream cylindrical nozzle anode, resulting in a plasma jet emerging into the surrounding outside atmosphere. Such direct current plasma torches are widely used in applications including plasma spraying, plasma gasification and waste conversion.

Conventional non-transferred arc plasma torches that were used in atmospheric plasma spraying technology usually operate with high currents (usually 300–800 A) and low output voltages (usually 30–80 V), depending on the applications. The voltage–current characteristics that are obtained during the operation of these arc plasma torches feature either sharp or slow drooping variations [1–3]. For example, the arc voltage decreases as the operating current increases when pure argon is used, which results in a decrease of the arc length inside the torch [1]. Moreover, the time-dependent voltage fluctuations during operation are usually in the range of 5 V to 20 V [2–4]. Large fluctuations of the plasma jet occur due to arc instabilities inside the torch, which significantly affect both the materials processing capability of the plasma jet and the electrode lifetime [3, 4]. Under these conditions, the length of a plasma jet of nitrogen, argon, hydrogen, helium or their mixtures discharging into an atmospheric environment is usually less than 200 mm, and experiences significant entrainment of the surrounding gas.

In order to improve the reproducibility and controllability of plasma processing technologies, many researchers have studied the stabilization of the arc discharge inside the direct current arc plasma torches. In 1995, a direct current non-transferred arc plasma torch that can generate a plasma jet of length over 400 mm into air was reported by Zhukov and coworkers from the Russian Academy of Science [1, 5]. Since then, several researchers have studied these plasma torches, often denoted as laminar plasma torches, in which the plasma jet length and the physical properties can be monotonically varied with the gas flow rate and output power. A research history of direct current laminar plasma torches is given in [6]. Chen, Pan and coworkers contributed valuable work on the two and 3D modelling of laminar plasma torches [7–10], predicting the internal pressure, velocity and temperature distribution and arc anode attachment behavior [11, 24], and comparing the properties of laminar plasma jets with the conventional arc plasma jets [12, 13] and with the experimental results [13–15].

Due to the significant difficulties in measuring the velocity and temperature distributions inside the plasma torch, numerical simulation is the most effective way to obtain fluid flow and heat transfer characteristics inside the plasma torch. In such models, the plasma gas is treated as a continuous, compressible, quasi-neutral fluid, and it is usually assumed that the plasma is in or close to the local thermodynamic equilibrium (LTE) state. An appropriate turbulence flow and the treatment of radiation transport, together with reliable data for the thermodynamic and transport properties are necessary requirements for the numerical modelling and simulation of the plasma flow within these torches.

Inside the plasma torch, the sudden expansion of the gas caused by the rapid heating by the arc increases its velocity and temperature by several orders of magnitude. As a result, the flow can become turbulent, especially as the plasma is injected into the surrounding environment. Appropriate consideration of turbulence within a plasma torch model requires special methods [16]. Turbulence modelling can be necessary to predict arc discharge shape and motion in some case [35]. In addition, realistic prediction of the particle trajectories and heating histories in thermal plasma spraying, especially when the powder is fed within the torch's inner

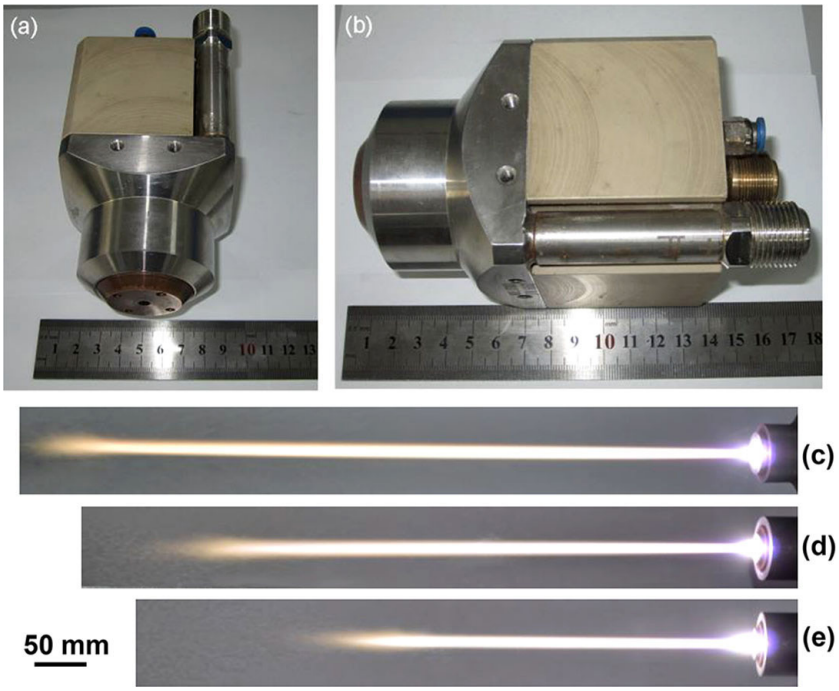

Figure 1. Photos of this plasma spray torch (a) and (b) and the long plasma jets in an atmospheric environment by using 70% nitrogen and 30% argon: (c) of $I = 160$ A and total gas flow rate of 8.5 SLPM [50], (d) of $I = 160$ A and total gas flow rate of 10 SLPM, (e) of $I = 160$ A and total gas flow rate of 14 SLPM [50]. [50] 2019 © Springer Science + Business Media, LLC, part of Springer Nature 2019. With permission of Springer.

channel, often depend on an appropriate method of modelling the turbulent flow.

Although the laminar flow regime has been assumed in some relevant modelling plasma torch modelling studies [17–21], Reynolds-averaged Navier–Stokes (RANS) turbulence models, which describe the time-averaged flow characteristics, have been most widely used for plasma torch modelling [19, 22–34]. These include the standard k–ε model, which has been the most commonly used (e.g. [22–24, 27, 32–34]), compared to other turbulence models [29, 33, 35, 36]. The renormalization group (RNG) RANS model improves predictions for high streamline curvature and strain rate, transitional flows, and wall heat and mass transfer, especially for low Reynolds-number flows [37, 38]. This makes the RNG model more realistic and reliable for a wider class of flows than the standard κ–ε model [29, 36], particularly for describing the flow inside arc torches. The large eddy simulation (LES) approach has been proposed as a method to capture the intricate dynamics in plasma spraying torches [39]. However, this approach requires highly accurate spatial and temporal discretization and it is often an order of magnitude or more expensive in terms of computing time than other methods [40], which makes LES impractical for repeated analyses and process monitoring.

A very common simulation treatment of radiative heat transfer in thermal plasma modelling is the net emission coefficient (NEC) method, which gives a good approximation for the radiation transport in the hottest area in most cases [35, 41]. A mole-fraction average of NECs of pure gases gives reasonable accuracy for gas mixture [42].

Thermodynamic and transport properties for pure plasma gases, including argon, helium, hydrogen, nitrogen, oxygen and air, can be obtained from the literature [43, 44, 48]. Both the simple interpolation mixing law and specific semi-empirical mixing rules are unsatisfactory and imprecise at low temperatures in plasmas in mixtures containing molecular gases, such as the argon–nitrogen mixtures considered in this paper [42, 45, 46]. Therefore, the properties for the mixture should be directly calculated. Additionally, it of often inappropriate to assume that the gases remain fully mixed. The combined diffusion coefficient method is a widely-used and relatively simple methods to treat diffusion in a mixture of two non-reacting gases [23, 47–49]. If the plasma gas can be assumed to be in the LTE state, the method gives the results equivalent to those from a full multicomponent treatment of diffusion [46, 47].

In this article, a novel direct current non-transferred arc plasma torch that can generate a jet over 350 mm in length into ambient air was studied. The internal flow field characteristics of this plasma torch were simulated in a 3D domain using a magnetohydrodynamic model (MHD) and the RNG turbulence model. The thermodynamic properties and the transport coefficients of nitrogen–argon mixture working gas were calculated for each mixture considered. The NEC approach was used to treat the radiative transport. The flow characteristics of nozzle outlet in this torch were predicted and compared to those of other atmospheric arc plasma torches.

2. The plasma torch performances

The novel plasma torch system consists of a power supply unit, a gas control unit and a plasma generation unit. The torch, which is comprised of a nozzle outlet, anode joint, cathode joint, auxiliary electrode joint and gas flow inlet, is the most crucial part of the plasma generation unit (figures 1(a) and (b)). The rated

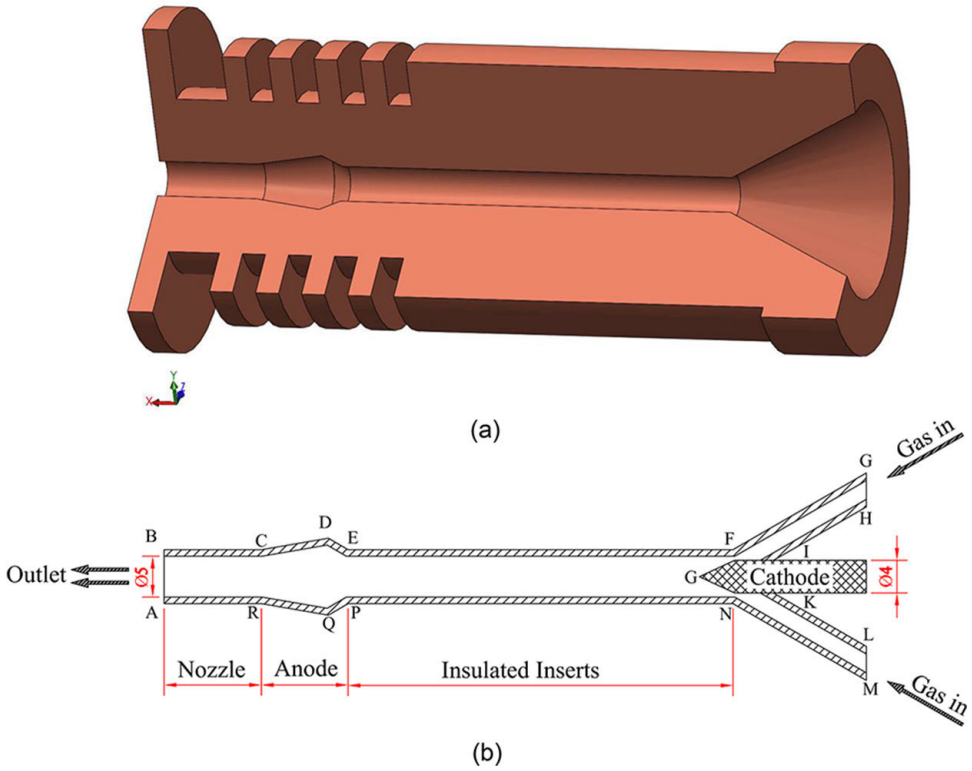

Figure 2. The plasma torch geometry: (a) 3D views of the inside of the torch, (b) the numerical calculation domain of cross-sectional and division of the boundaries.

Table 1. Boundary conditions in simulation.

Defined region	Specified boundary	T(K)	A	V(SLPM)	P(atm)	ϕ
Outlet	AB	$\partial T/\partial n = 0$	$\partial A_i/\partial n = 0$	$\partial V_i/\partial n = 0$	1.0	$\partial\phi/\partial n = 0$
Anode	CDE/PQR	$h_w(T - T_w)$	$\partial A_i/\partial n = 0$	0	$\partial P/\partial n = 0$	0
Wall	BC/EFG/MNP/AR	$h_w(T - T_w)$	—	—	—	—
Cathode	HIGKL	$T(r)$	$\partial A_i/\partial n = 0$	0	$\partial P/\partial n = 0$	$J(r)$
Gas in	GH/LM	300	0	8.5/10/14	1.1	$\partial\phi/\partial n = 0$

power of the torch is 30 kW. The input gas is a mixture of 70% nitrogen and 30% argon in volume. The plasma jet of length ranging from 100 to 720 mm can be generated by controlling the gas input rate ranging from 8.5 to 15 SLPM and the output power from 8.5 to 28 kW. The length of the plasma jets generally increases with output power and gas flow rate. The maximum length of the long plasma jet reaches 720 mm at a current of 160 A and a gas flow rate of 8.5 SLPM. The voltage fluctuation values are confined within a range between $\pm$0.5 V and $\pm$2 V [50]. It provides a new selection of atmospheric plasma spray methods with a high controllability and stability [51, 52].

Photos of the plasma torch are shown in figures 1(a) and (b). Figure 1(c) shows the long plasma jet in the atmospheric environment at a current of 160 A and total gas flow rate of 8.5 SLPM consisting of 70% nitrogen and 30% argon by volume. Figure 1(d) shows the long plasma jet in the atmospheric environment at a current of 160 A and total gas flow rate of 10 SLPM consisting of 70% nitrogen and 30% argon by volume. Figure 1(e) shows the long plasma jet in the atmospheric environment at a current of 160 A and total gas flow rate of 14 SLPM consisting of 70% nitrogen and 30% argon by volume. It can be deduced that the length of plasma jet is decreased by the increasing of gas flow rate at a constant current in experiment. These three different parameters are used as the operational conditions in the following numerical simulations.

3. Modelling approaches

3.1. Model assumptions

The following assumptions are adopted,

- The plasma flow inside the plasma torch is quasi-steady.
- The self-induced magnetic field in the arc plasma is negligible.
- The plasma gas is treated as a single continuous fluid characterized by a single temperature for all species. The transport properties are functions of temperature only.
- The plasma flow is in a local thermodynamic equilibrium (LTE).
- Gravitational effect is considered negligible.
- The working gas at the gas inlet is injected in the axial direction, without any swirling velocity component.

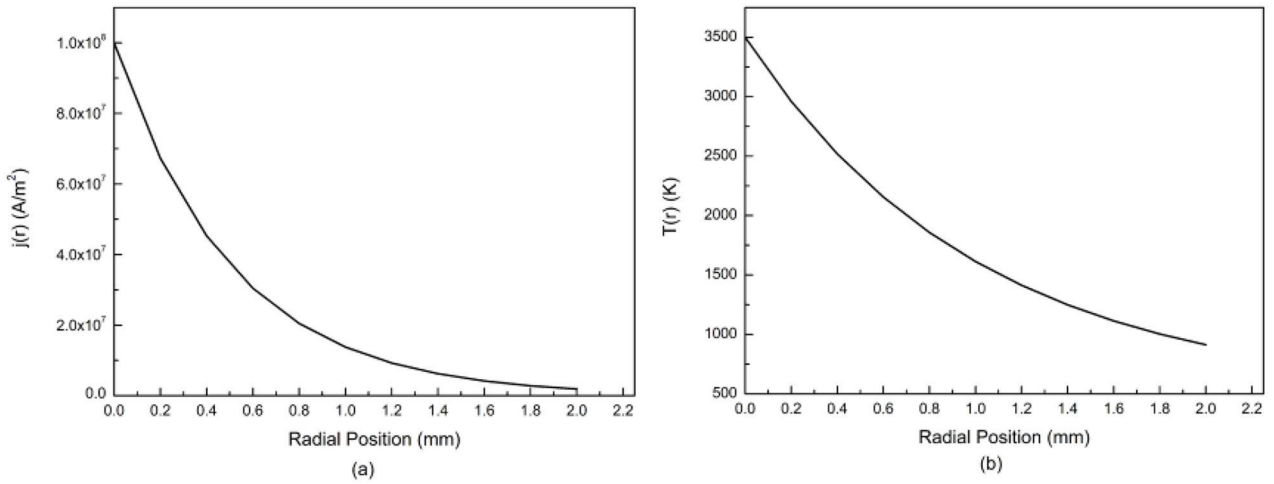

Figure 3. Radial profiles of assumed current density (a) and temperature (b) over the cathode tip used as boundary conditions.

3.2. Governing equations and boundary conditions

According to above assumptions, the governing equations for the 3D plasma flow can be written in (r, θ, z) coordinates as follows:

- Continuity equation:

$$\frac{1}{r}\frac{\partial}{\partial r}(r\rho v_r)+\frac{1}{r}\frac{\partial}{\partial \theta}(\rho v_\theta)+\frac{\partial}{\partial z}(\rho v_z)=0. \tag{1}$$

- Momentum conservation equations:

$$\begin{aligned}\rho(v_r\tfrac{\partial v_r}{\partial r}+\tfrac{v_\theta}{r}\tfrac{\partial v_r}{\partial \theta}+v_z\tfrac{\partial v_r}{\partial z})&=-\tfrac{\partial p}{\partial r}+\tfrac{\partial}{\partial r}[2\mu_{eff}\tfrac{\partial v_r}{\partial r}]\\&+\tfrac{1}{r}\tfrac{\partial}{\partial \theta}[\mu_{eff}(\tfrac{1}{r}\tfrac{\partial v_r}{\partial \theta}+\tfrac{\partial v_\theta}{\partial r}-\tfrac{v_\theta}{r})]\\&+\tfrac{\partial}{\partial z}[\mu_{eff}(\tfrac{\partial v_r}{\partial z}+\tfrac{\partial v_z}{\partial r})]\\&+\tfrac{2(\mu+\mu_t)}{r}(\tfrac{\partial v_r}{\partial r}-\tfrac{1}{r}\tfrac{\partial v_\theta}{\partial \theta}-\tfrac{v_r}{r})+\rho\tfrac{v_\theta^2}{r}+F_r\end{aligned} \tag{2}$$

$$\begin{aligned}\rho(v_r\tfrac{\partial v_\theta}{\partial r}+\tfrac{v_\theta}{r}\tfrac{\partial v_\theta}{\partial \theta}+v_z\tfrac{\partial v_\theta}{\partial z})&=-\tfrac{1}{r}\tfrac{\partial p}{\partial \theta}\\&+\tfrac{\partial}{\partial r}[\mu_{eff}(\tfrac{\partial v_\theta}{\partial r}-\tfrac{v_\theta}{r}+\tfrac{1}{r}\tfrac{\partial v_r}{\partial \theta})]+\tfrac{1}{r}\tfrac{\partial}{\partial \theta}[2\mu_{eff}(\tfrac{1}{r}\tfrac{\partial v_\theta}{\partial r}+\tfrac{v_r}{r})]\\&+\tfrac{\partial}{\partial z}[\mu_{eff}(\tfrac{\partial v_\theta}{\partial z}+\tfrac{1}{r}\tfrac{\partial v_z}{\partial \theta})]\\&+\tfrac{2(\mu+\mu_t)}{r}(\tfrac{1}{r}\tfrac{\partial v_r}{\partial \theta}+\tfrac{\partial v_\theta}{\partial r}-\tfrac{v_\theta}{r})-\rho\tfrac{v_r v_\theta}{r}+F_\theta\end{aligned} \tag{3}$$

$$\begin{aligned}\rho(v_r\tfrac{\partial v_z}{\partial r}+\tfrac{v_\theta}{r}\tfrac{\partial v_z}{\partial \theta}+v_z\tfrac{\partial v_z}{\partial z})&=-\tfrac{\partial p}{\partial z}\\&+\tfrac{1}{r}\tfrac{\partial}{\partial r}[r\mu_{eff}(\tfrac{\partial v_z}{\partial r}+\tfrac{\partial v_r}{\partial z})]+\tfrac{1}{r}\tfrac{\partial}{\partial \theta}[\mu_{eff}(\tfrac{1}{r}\tfrac{\partial v_z}{\partial \theta}+\tfrac{\partial v_\theta}{\partial z})]\\&+\tfrac{\partial}{\partial z}[2\mu_{eff}\tfrac{\partial v_z}{\partial z}]+F_z.\end{aligned} \tag{4}$$

- Energy conservation equation:

$$\begin{aligned}\rho C_p(v_r\frac{\partial T}{\partial r}+\frac{v_\theta}{r}\frac{\partial v_z}{\partial \theta}+v_z\frac{\partial T}{\partial z})&=\nabla\cdot(\kappa_{eff}\nabla T)\\&+\frac{j_r^2+j_\theta^2+j_z^2}{\sigma}+\frac{5}{2}\frac{k_B}{e}j\cdot\nabla T-4\pi\varepsilon_r.\end{aligned} \tag{5}$$

- Electric potential:

$$\frac{1}{r}\frac{\partial}{\partial r}(r\sigma\frac{\partial \phi}{\partial r})+\frac{1}{r^2}\frac{\partial}{\partial \theta}(\sigma\frac{\partial \phi}{\partial \theta})+\frac{\partial}{\partial z}(\sigma\frac{\partial \phi}{\partial z})=0.$$

In equations (2)–(4), the components of the Lorentz force are given by:

$$\mathbf{F}=\mathbf{j}\times\mathbf{B}. \tag{7}$$

In equation (5), the electric current density vector relates to the electric field intensity and electric potential according to:

$$\mathbf{j}=\boldsymbol{\sigma}\mathbf{E}=-\boldsymbol{\sigma}\nabla\phi. \tag{8}$$

The magnetic induction intensity vector can be calculated using:

$$\mathbf{B}=\nabla\times\mathbf{A} \tag{9}$$

where

$$\nabla^2\cdot\boldsymbol{A}=-\mu_0\cdot\mathbf{j} \tag{10}$$

which is explicitly solved using:

$$A=\frac{\mu_0}{4\pi}\int_v\frac{j}{r}dV. \tag{11}$$

- Turbulence model transport equations [38, 53, 54]:

$$\rho\left(v_r\frac{\partial k}{\partial r}+v_\theta\frac{\partial k}{\partial \theta}+v_z\frac{\partial k}{\partial z}\right)=\nabla\cdot(\alpha_k\mu_{eff}\nabla k)+G_k-\rho\varepsilon-Y_M \tag{12}$$

$$\begin{aligned}\rho\left(v_r\frac{\partial \varepsilon}{\partial r}+v_\theta\frac{\partial \varepsilon}{\partial \theta}+v_z\frac{\partial \varepsilon}{\partial z}\right)&=\nabla\cdot(\alpha_\varepsilon\mu_{eff}\nabla\varepsilon)\\&+C_{1\varepsilon}G_k\frac{\varepsilon}{k}-C_{2\varepsilon}\rho\frac{\varepsilon^2}{k}-R_\varepsilon.\end{aligned} \tag{13}$$

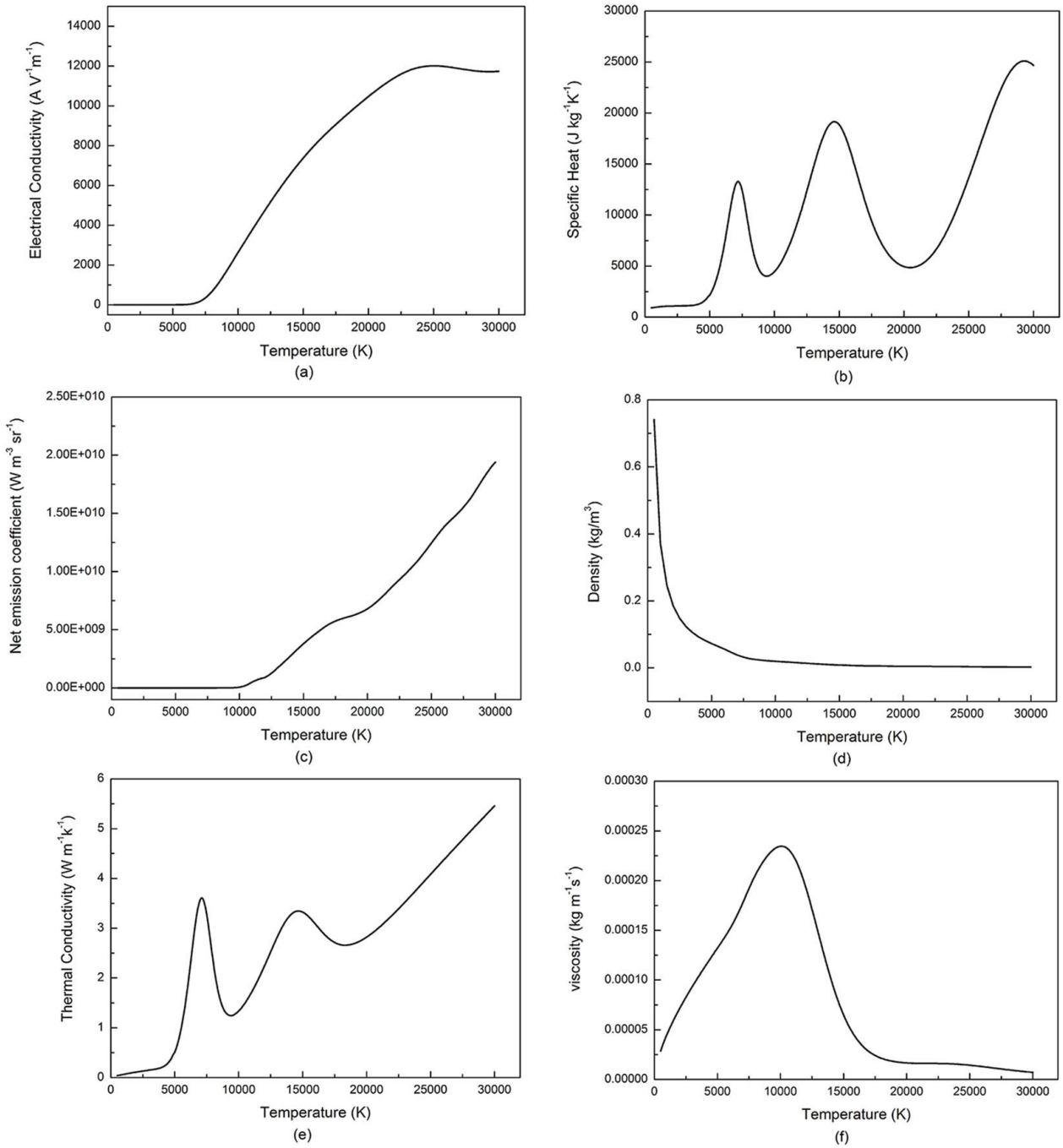

Figure 4. Thermodynamic and transport properties of plasma gas composed of 70% nitrogen and 30% argon mixture by volume: (a) electrical conductivity; (b) specific heat; (c) net emission coefficient; (d) density; (e) thermal conductivity; (f) viscosity.

In equations (12) and (13), G_k represents the generation of turbulence kinetic energy due to the mean velocity gradients, and Y_M represents the contribution of the fluctuating dilatation in compressible turbulence to the overall dissipation rate. The quantities α_k and α_ε, respectively the inverse effective Prandtl numbers for k and ε are both set equal to 1.393. $C_{1\varepsilon}$ and $C_{2\varepsilon}$ are set equal to 1.42 and 1.68. The main difference between the RNG and the standard k–ε model lies in the additional term of the turbulent dissipation equation given by [37, 38]:

$$R_\varepsilon = \frac{C_\mu \rho \eta^3 (1-\eta/\eta_0)}{1+\beta\eta^3} \cdot \frac{\varepsilon^2}{k} \tag{14}$$

where $\eta_0 = 4.38$, $\beta = 0.012$, $C_\mu = 0.0845$. The effective viscosity is given by:

$$\mu_{eff} = \mu + \mu_t \tag{15}$$

$$\mu_t = \rho C_\mu \frac{k^2}{\varepsilon}. \tag{16}$$

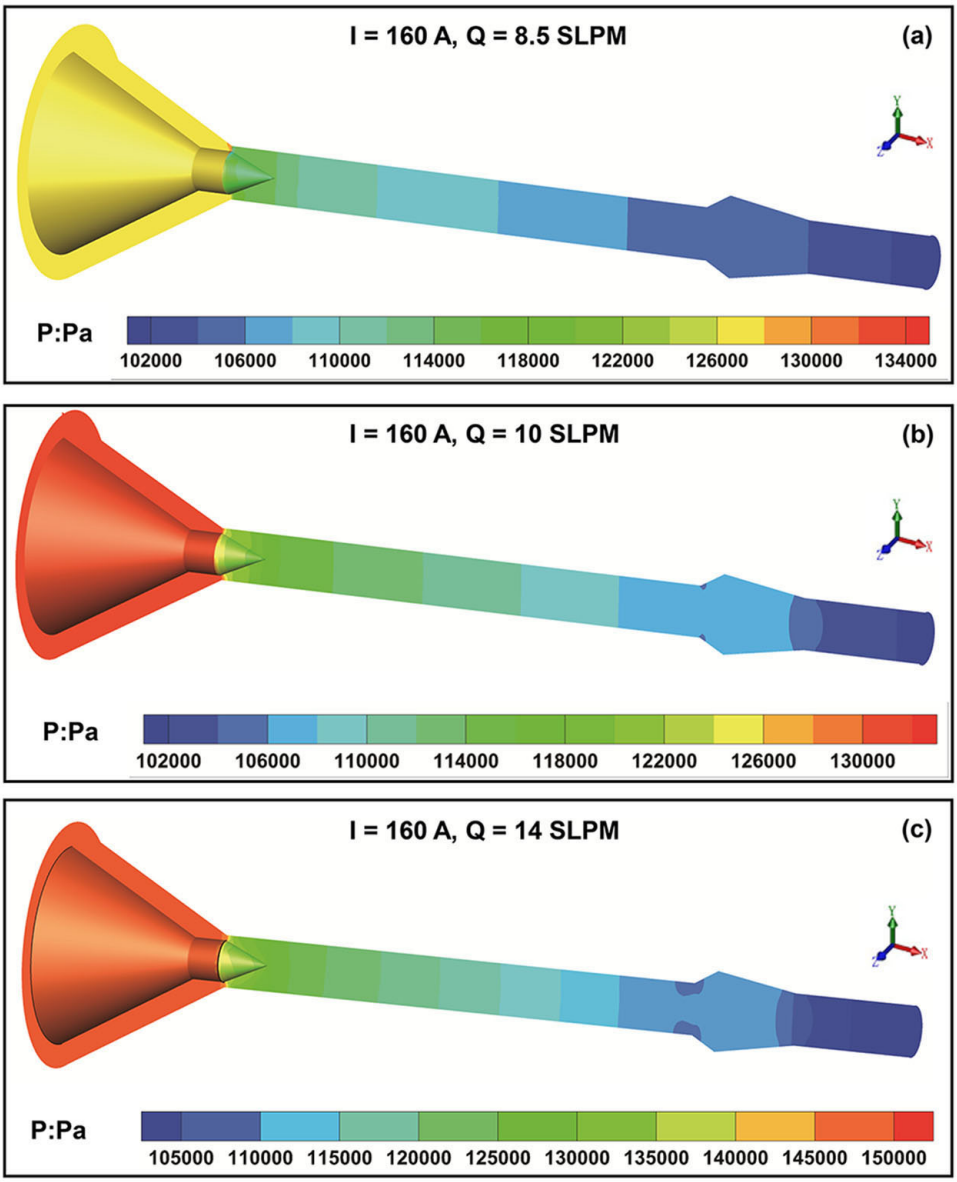

Figure 5. Pressure distributions in the cross-sectional planes inside the plasma torch: (a) of $I = 160$ A and total gas flow rate of 8.5 SLPM; (b) of $I = 160$ A and total gas flow rate of 10 SLPM; (c) of $I = 160$ A and total gas flow rate of 14 SLPM.

The governing equations are solved by ANSYS Fluent.16.0 using the SIMPLE algorithm [38]. FLUENT has the basic capabilities to solve the conservation equations of continuity, momentum, and energy. The equations and relations to determine the electric potential, the magnetic vector potential, the electric field, the magnetic induction vector, and the electric current density vector are solved via FLUENT's user-defined memory (UDM), user-defined scalar (UDS), and user-defined functions (UDF) [38, 55].

3.3. Computational domain and boundary conditions

The diameters of the nozzle outlet and tungsten rod cathode are 5 mm and 4 mm, respectively. The insulated inserts are assembled with several insulating rings to extend and constrict the arc column in a cylindrical channel. The direct current non-transferred arc is established between a cylindrical cathode with conical tip and a water-cooled anode with a trumpet-liked shape. The plasma flow is induced along the cylindrical channel and injected into ambient environment to form a long plasma jet.

The schematic diagrams of the internal flow channel of the plasma torch and the numerical calculation domain are shown in figure 2. The boundaries of the computational domain are divided into five different regions to allow the specification of boundary conditions, which are listed in table 1. The number of nodes in the computational mesh is 360 020 and the number of iterations required for a converged result is 528 400.

At the circular ring inlet boundary, the radial velocity is assumed to be zero, and the pressure is set to 111.3 kPa. The total gas flow rates are set to 8.5 SLPM, 10 SLPM and 14 SLPM, respectively, and the working gas is a mixture of

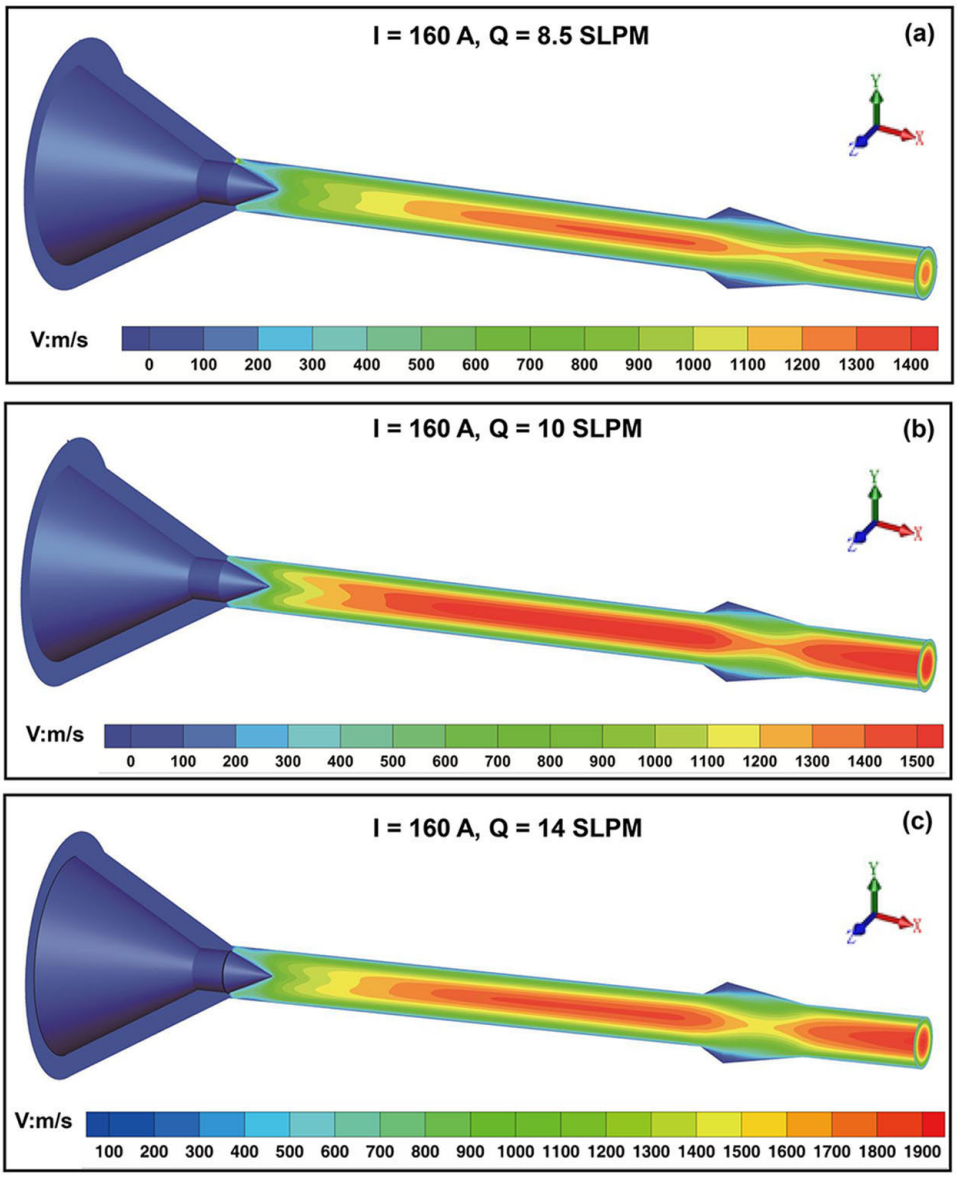

Figure 6. Velocity distributions in the cross-sectional planes inside the plasma torch: (a) of $I = 160$ A and total gas flow rate of 8.5 SLPM; (b) of $I = 160$ A and total gas flow rate of 10 SLPM; (c) of $I = 160$ A and total gas flow rate of 14 SLPM.

70% nitrogen and 30% argon by volume. The outside of the anode and wall boundaries are assumed to be water-cooled satisfying the condition:

$$-k\left(\frac{\partial T}{\partial r}\right)_w = h_w\,(T_W - T_\infty) \tag{17}$$

where the heat transfer coefficient h_w is $1.0 \times 10^5\,\mathrm{W\,m^{-2}\,K^{-1}}$, and the T_w is the reference surface temperature of the anode of 500 K [32, 40, 57, 63].

The boundary condition on the anode surface for the electromagnetic field considers zero electrical potential. Current density and temperature distributions are defined over the cathode rod tip [16]. It is found that the value of j_r has no significant effect on the temperature and velocity distributions at the nozzle exit, as the process of heat and momentum exchange through the downstream of the plasma torch channel can eliminate the bias value [29, 34]. The current density (figure 3(a)) and the temperature distribution (figure 3(b)) at the cathode tip are modelled using [56]:

$$j(r) = J_{max}\exp(-(r/R_c)^{n_c}) \tag{18}$$

and

$$T(r) = T_w + T_c\exp\left(-\left(\frac{r}{2R_c}\right)^{n_c}\right). \tag{19}$$

The value of the maximum current density J_{max} is chosen to ensure the integral of $j(r)$ over the cathode is equal to the applied current; r_h is the radius of the hottest part of the cathode tip, and r is the radial coordinate measured from the torch axis ($r^2 = x^2 + y^2$), and together with J_{max}; n_c specifies the shape of current density profile [29, 56], which is set to be 1 in this work. R_c is chosen to ensure that the integration of $j(r)$ over the cathode surface equals to the total applied current, which is set to be 0.51 mm in this work. The maximum value

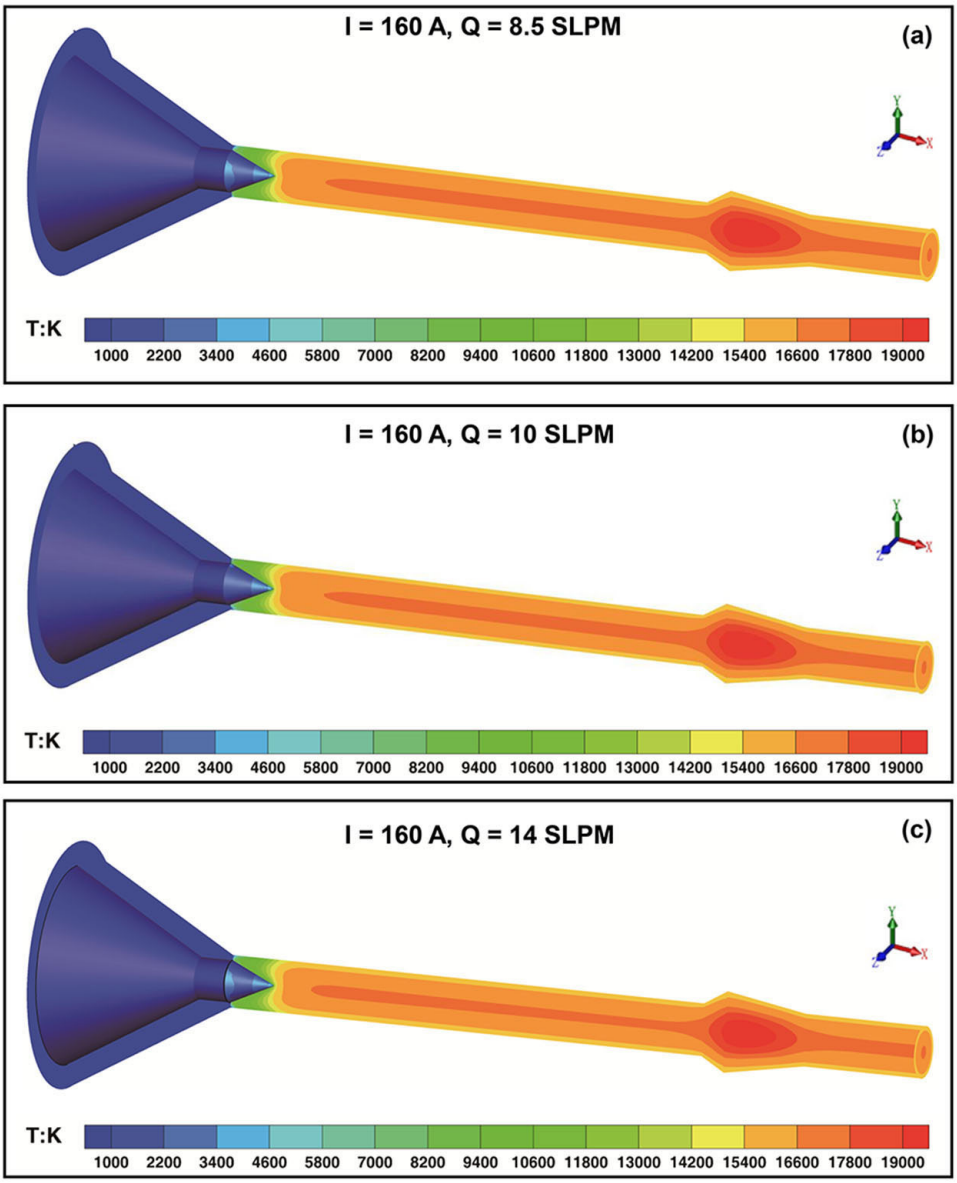

Figure 7. Temperature distributions in the cross-sectional planes inside the plasma torch: (a) of $I = 160$ A and total gas flow rate of 8.5 SLPM; (b) of $I = 160$ A and total gas flow rate of 10 SLPM; (c) of $I = 160$ A and total gas flow rate of 14 SLPM.

of current density is assumed to be on the order of 10^8 A m^{-2} for commercial plasma spray torches operating between 100 A and 800 A [40]. For the free-burning arc operating under a working current of 200 A at atmospheric pressure [56], J_{max} was defined to be 1.2×10^8 A m^{-2}. Based on the above references, in this case, J_{max} is set to 1.0×10^8 A m^{-2} for a working current of 160 A. T_w and T_c are set to 500 K and 3000 K.

An artificially high electrical conductivity of the level of 10^4 S m^{-1} at the beginning of the simulations that was imposed on a layer of 0.1 mm thickness along the anode wall [7, 24, 30, 32, 34, 57, 63]. This artificially high-conducting allows a new arc root to be formed if the arc is close enough to the inside surface of the anode. This high-conducting region is required, given the adoption of the LTE assumption, to ensure the flow of electrical current from the plasma to the anode [32, 34, 57]. This high value slightly decreases the size of the anode spot and exerts little effects on the final results [24, 57].

3.4. Thermodynamic and transport properties

The calculation of radiative transport, thermodynamic and transport properties are required to complete the plasma flow model. The density, viscosity, specific heat, electrical conductivity and thermal conductivity are plotted for a pressure of 101.325 kPa and the temperature range from 300 K to 30 000 K (figures 4(a)–(f)). These were calculated using the methods presented by Murphy [46–49, 58]. The net emission coefficients are obtained using a mole-fraction weighted averaged of the data of Cram [59] for argon and Ernst *et al* for nitrogen [60], for an absorption length of 1 mm. The data of Ernst *et al*

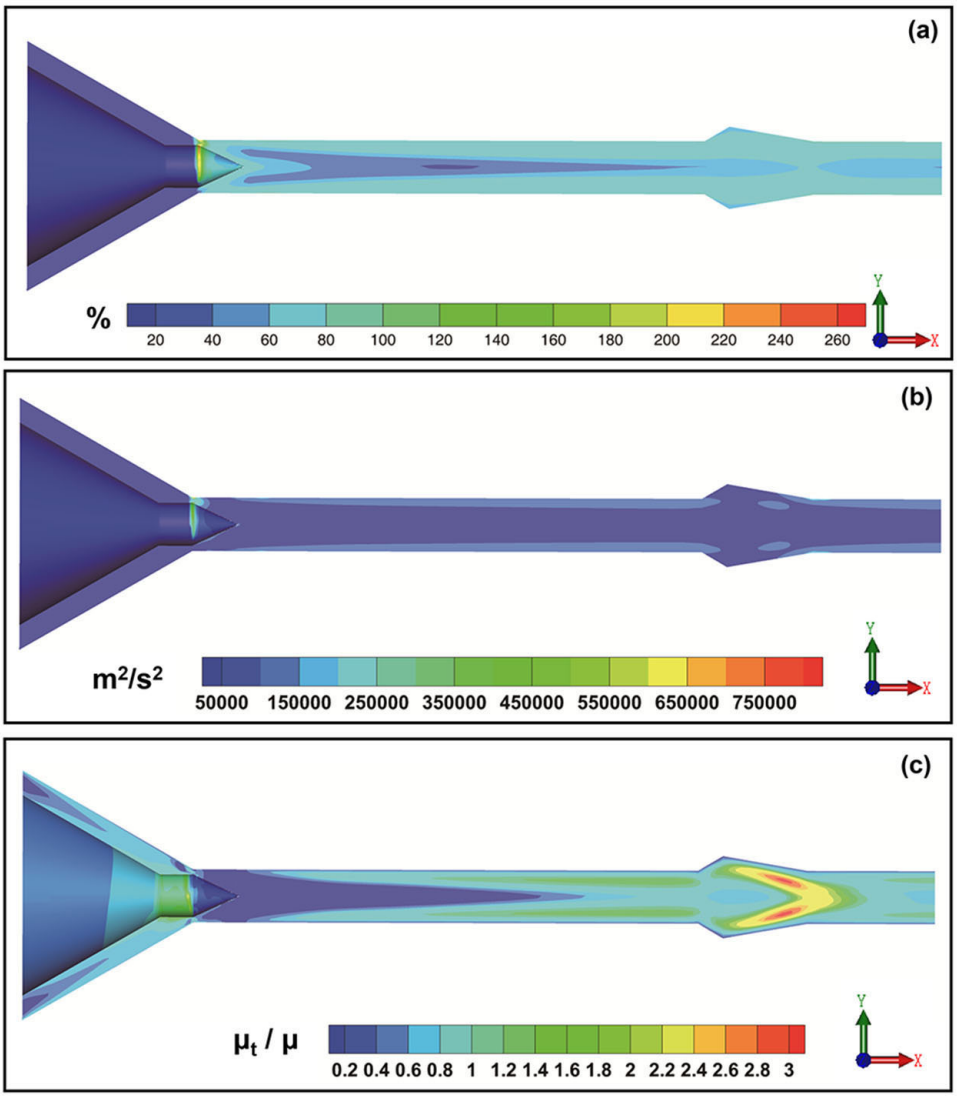

Figure 8. Turbulent intensity (a), turbulent kinetic energy (b), turbulent viscosity ratio μ_t/μ (c) distributed in the perpendicular longitudinal plane along the torch ($I = 160$ A, $Q = 8.5$ SLPM).

is given for an absorption length of 3 mm; their given value is multiplied by 1.5 to adjust for this discrepancy [61].

4. Simulation results

4.1. Flow fields inside the plasma torch

The obtained pressure, velocity and temperature fields within the plasma torch are presented in figures 5–7, respectively. The pressure inside the torch decreases in the direction of flow from the gas inlet to the outlet, with a high-pressure area near the cathode at three different operational conditions in figure 5. A narrow circular gap between the boundary of cathode and the channel wall generates large gradients of pressure. The maximum pressure is increased by the increasing of total gas flow rate from 8.5 SLPM (figure 5(a)), 10 SLPM (figure 5(b)) to 14 SLPM (figure 5(c)). However, the pressure distributions at the torch nozzle are in the range of 102 kPa to 105 kPa under the three different conditions.

The velocity distributions are shown in figure 6. The flow is greatly accelerated when passing through the anode region and forms two distinct vortexes upstream and downstream of the anode. The more intense vortex is located close to the nozzle exit; the flow velocity is about one order of magnitude greater than that near the cathode tip. The maximum velocity at the nozzle exit reaches 1474.5 m s^{-1}, 1506.8 m s^{-1} and 2024 m s^{-1} at three different gas flow rates in figures 6(a)–(c), respectively.

A distinct arc column region with temperature over 15 000 K extends from near the tip of the cathode to the anode area and expands appreciably as it enters the anode region. The high-temperature region contracts as it leaves the anode region, forming a hot jet that emerges from the nozzle exit (figure 7). However, at these three different gas flow rates, the predicted maximum temperature in the center of anode region are in the range of 19 300 K to 19 530 K. The experimental arc voltages of the three gas flow conditions are 148.8 ± 0.5 V, 150.9 ± 1 V and 157.5 ± 0.5 V (by TPS-2000

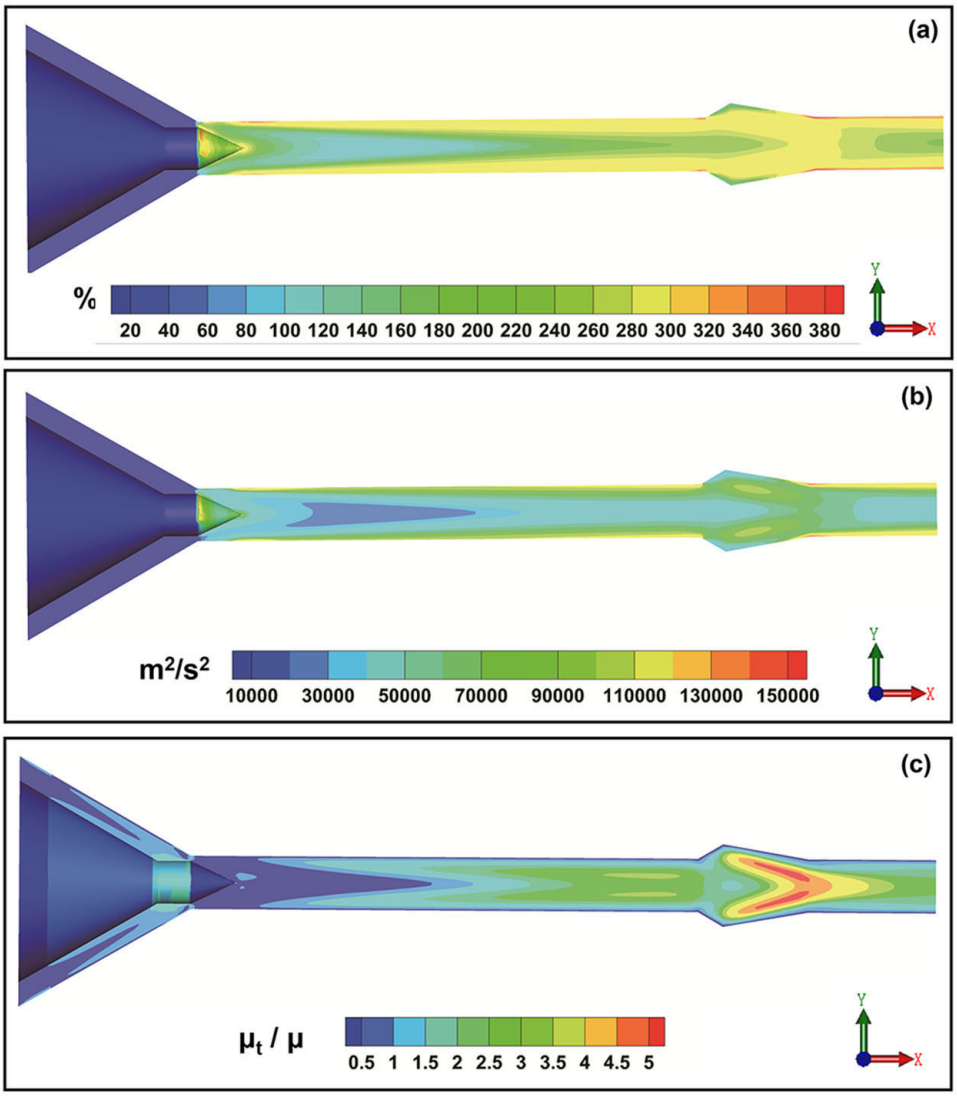

Figure 9. Turbulent intensity (a), turbulent kinetic energy (b), turbulent viscosity ratio μ_t/μ (c) distributed in the perpendicular longitudinal plane along the torch (I = 160 A, Q = 10 SLPM).

probe, Tektronix Inc. USA) [50], respectively. In the simulation result, the arc column is expanded in the anode area according to the temperature distribution and it cannot find a very clear arc attachment position. The trumpet-like structure of the anode is situated close to the nozzle exit. The expansion of the arc column diminishes the compression effect of the cold boundary layer on the arc column, which allow the arc movement favor in a steady model [3, 62]. This indicated that the arc attachment root at the anode is not immediately dragged downstream by the flow, as occurs in conventional non-transferred arc plasma torches with linear channel structure (e.g. Sulzer F4 Torch or Praxair SG-100 Torch), so the periodic variation in arc length and therefore arc voltage that occur in such torches does not occur.

4.2. Turbulent transport predicted inside the plasma torch

The specially designed trumpet-like anode has a significant effect on the flow field inside the torch channel. The internal flow is separated into a *primary channel flow* and a *secondary edge flow* along the anode surface. As the *primary flow* is separated at the extended edge of anode wall, the velocity of the *secondary flow* at the bottom of the anode is 200 to 400 m s^{-1} in figure 6, which is significantly lower than that of the *primary channel flow*. A decreasing gradient of turbulent intensity from the *secondary flow* to the *primary flow* is evident in figures 8–10 under these three different conditions by using the RNG turbulent model. The distributions of higher turbulent intensity locate at the boundary of torch wall.

The turbulent kinetic energy (k) and turbulent viscosity ratio (μ_t/μ) distributions all show a high gradient from the tip of cathode to anode in the perpendicular planes of the torch from figures 8–10. A very high turbulent viscosity ratio region refers to turbulence dominated flow and a low value of this ratio represents regions of laminar flow. The maximum turbulent viscosity is increased by the increasing of total gas flow rate from 8.5 SLPM (figure 8), 10 SLPM (figure 9) to 14 SLPM (figure 10).

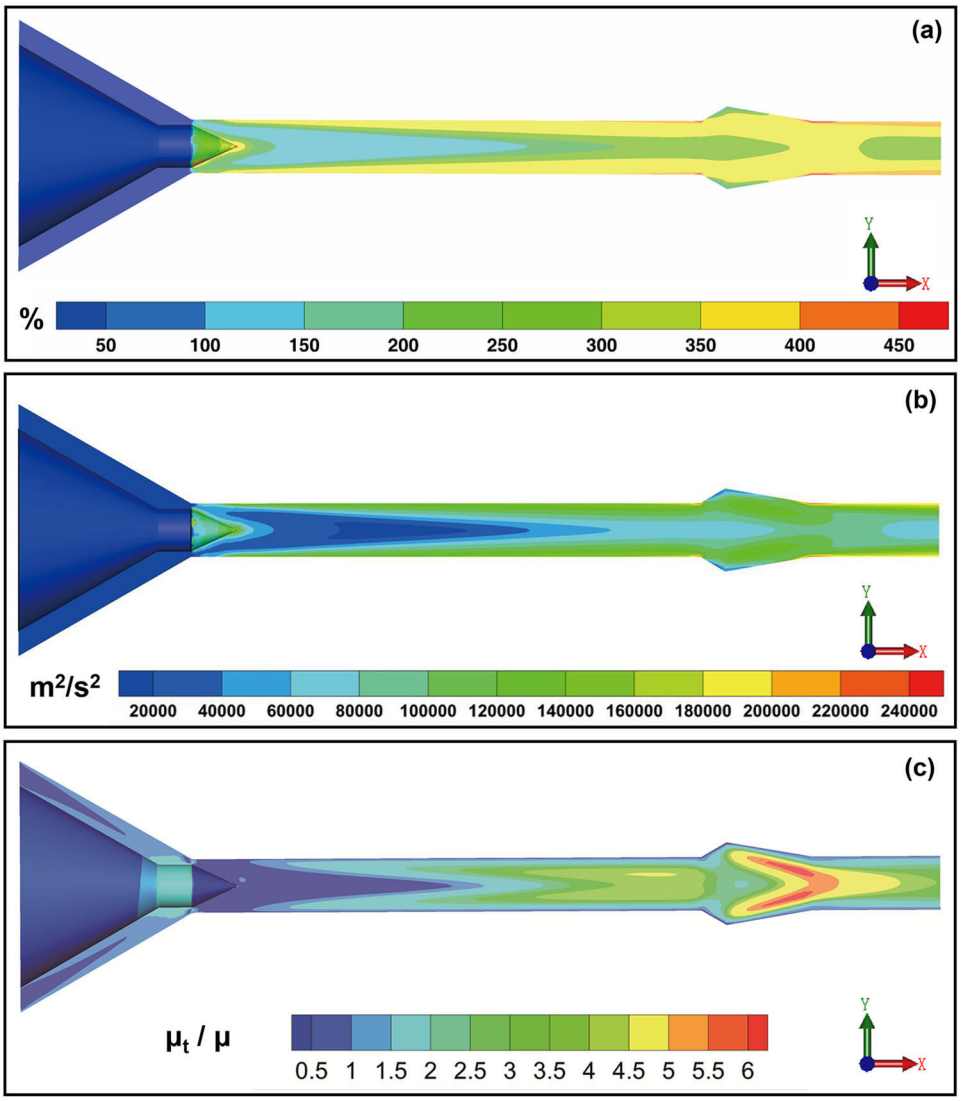

Figure 10. Turbulent intensity (a), turbulent kinetic energy (b), turbulent viscosity ratio μ_t/μ (c) distributed in the perpendicular longitudinal plane along the torch (I = 160 A, Q = 14 SLPM).

4.3. Electric and magnetic distributions inside the plasma torch

The electrical potential under these three different conditions are presented in figures 11(a), (b) and 12(a), respectively. The axial component of the magnetic potential inside the torch at the total gas flow rate of 14 SLPM is shown in figure 12(b). The predicted maximum arc voltage is 150 V, 152 V and 158 V at the total gas flow rate of 8.5 SLPM, 10 SLPM and 14 SLPM, respectively. The arc voltage in this plasma torch is almost three times that of other conventional non-transferred arc plasma torches operating at the same output power. The arc voltage comparisons between the experiment and the simulation are listed in table 2.

The electrical current density along the z-direction are shown in figure 13. A high electrically conducting path connects the tip of cathode and the anode. The arc is predicted to attach the edge of the anode region and distributed in a circular area at the steady model. The anode erosion occurred at the downstream edge, and no erosion was observed at other positions after twenty hours' of operation in the experimental tests.

4.4. Flow characteristics at the torch nozzle

Figure 14 presents the temperature and velocity distributions at the torch nozzle under three different conditions and comparing with other atmospheric arc plasma torches. Figures 14(a)–(c) show the velocity contours that are combined with the flow vector at the torch nozzle in three different gas flow rates, respectively. The flow velocity is over 1000 m s^{-1} across almost 70% of the cross-sectional area. The obtained maximum velocity at the torch nozzle in this method is 1474.5 m s^{-1}, 1506.8 m s^{-1} and 2024 m s^{-1}, respectively.

The velocity and temperature at torch nozzle are compared with those predicted by simulations of three different non-transferred arc plasma torches in figures 14(d) and (e). These are two widely-used commercial plasma torches and one laminar plasma torch, namely:

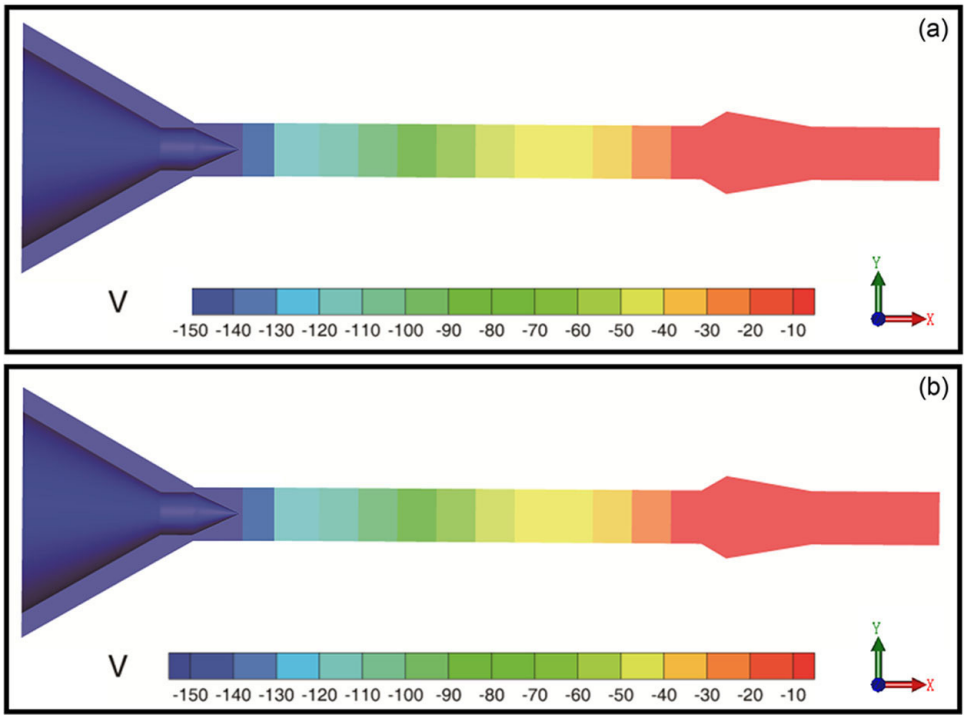

Figure 11. Electric potential in the perpendicular longitudinal plane along the plasma torch at a constant current of 160 A: (a) total gas flow rate of 8.5 SLPM, (b) total gas flow rate of 10 SLPM.

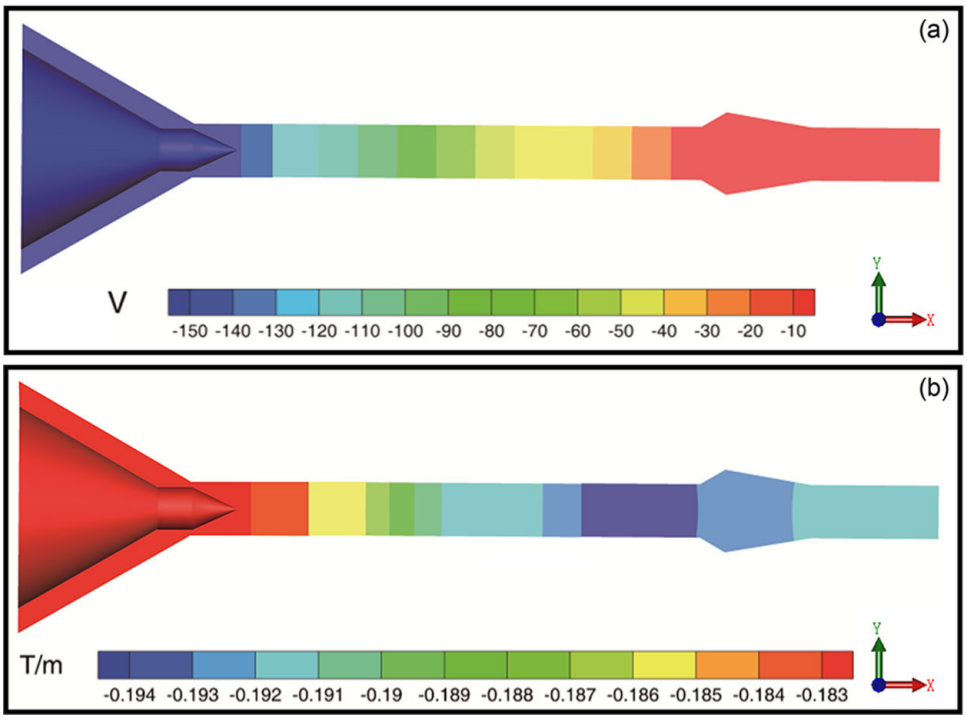

Figure 12. Electric potential (a) and axial component of the magnetic vector potential (b) in the perpendicular longitudinal plane along the plasma torch at the total gas flow rate of 14 SLPM and current of 160 A.

Table 2. The arc voltage comparisons between the experiment and the simulation.

Operation conditions ($I = 160$ A)	Experiment	Simulation (V)
$Q = 8.5$ SLPM	148.8 ± 0.5 V	150
$Q = 10$ SLPM	150.9 ± 1 V	152
$Q = 14$ SLPM	157.5 ± 0.5 V	158

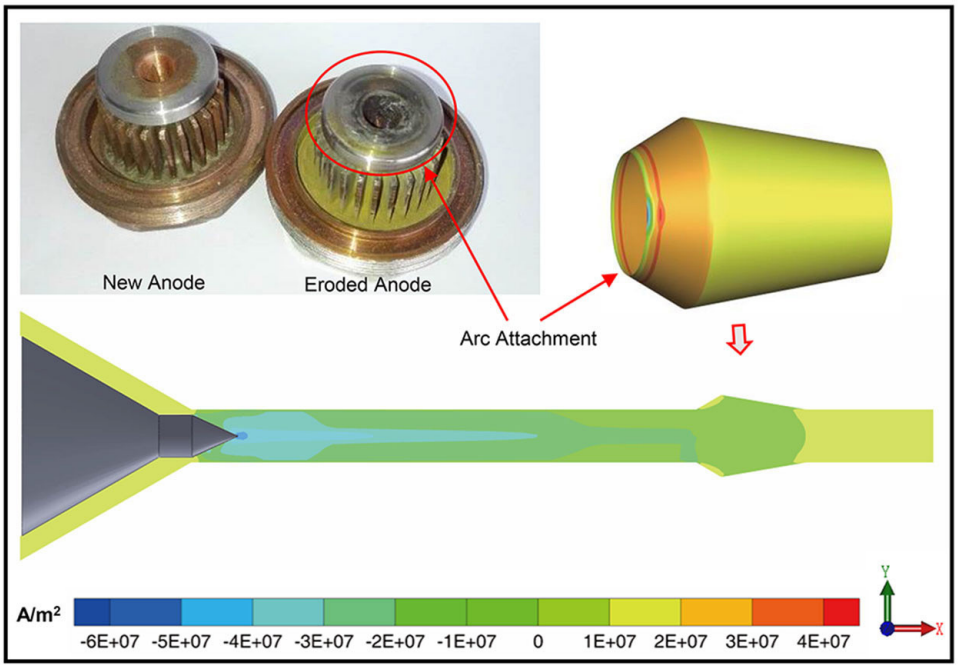

Figure 13. Axial component of the electric current density distribution and predicted arc attachment compared to the experimentally-obtained eroded anode ($I = 160$ A, $Q = 14$ SLPM).

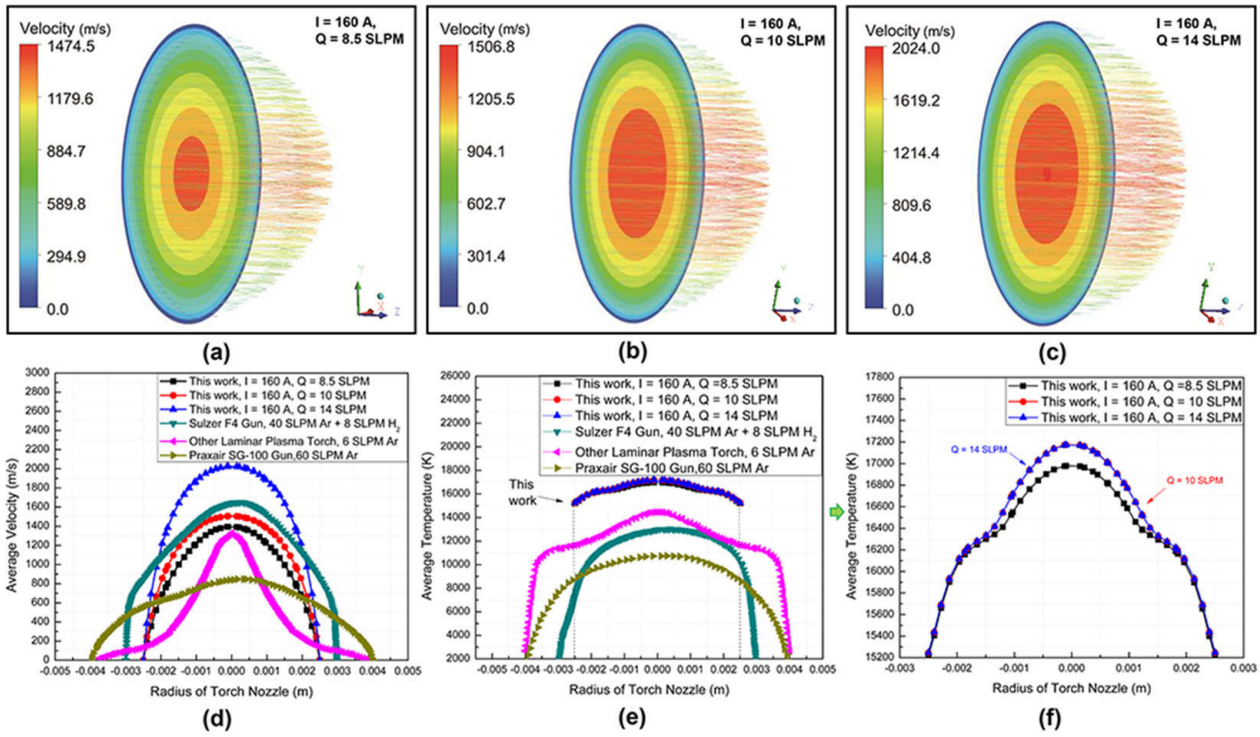

Figure 14. The velocity and flow vector in the cross-section of the nozzle exit: (a) $I = 160$ A and total gas flow rate of 8.5 SLPM; (b) $I = 160$ A and total gas flow rate of 10 SLPM; (c) $I = 160$ A and total gas flow rate of 14 SLPM; azimuthally averaged flow velocity (d) and temperature (f) within the three different conditions compared to values obtained in other atmospheric arc plasma torches (e).

Table 3. The comparisons of outlet maximum velocity and temperature between this works and other arc plasma torches.

Type	Maximum velocity (m s^{-1})	Maximum temperature (K)
This work, $Q = 8.5$ SLPM	1474.5	16979.8
This work, $Q = 10$ SLPM	1506.8	17159.2
This work, $Q = 14$ SLPM	2024.0	17172.8
Xu *et al* [9]	1330.7	14453.2
Trelles *et al* [63]	846.4	10745.9
Guo *et al* [34]	1650.7	13031.5

- Laminar plasma torch from the Chinese Academy of Science (Pan and Xu *et al*, *pure argon*, $Q = 5.7$–6 slpm, *nozzle diameter* = 8 mm, $I = 170$ A, 10 kW [9, 31]).
- Praxair SG-100 torch (Trelles *et al*, *pure argon*, $Q = 60$ slpm, *nozzle diameter* = 8 mm, $I = 800$ A, 32 kW [63]).
- Sulzer-Metco F4 Gun (Guo *et al*, $Q = 40$ slpm $Ar + 8$ slpm H_2, *nozzle diameter* = 6 mm, $I = 400$ A, 24 kW [34]).

The two commercial dc non-transferred arc plasma torches usually operate at a minimum gas flow rate of 30 SLPM and at output powers of 18 to 60 kW, the voltage-current characteristics show the higher currents (usually 300–800 A) and lower voltages (usually 30–80 V) by using working gases such as argon, nitrogen, helium, hydrogen or their mixtures [4, 64, 65]. The jet length cannot reach over 200 mm discharging into an air atmosphere because of the intense entrainment of air. The other type of laminar plasma torch can generate a laminar plasma jet of length 200–500 mm in an atmospheric air under different working conditions [9, 31]. The comparisons of maximum velocity and temperature at the torch nozzle between this works and other arc plasma torches are listed in table 3.

Comparing with the obtained values of other simulation results, this novel plasma spray torch produces a jet length of over 350 mm into atmospheric air and is predicted to have much higher velocity and temperature at the nozzle exit when operated at an output power of 25.4 kW and total gas flow rate of 14 SLPM by using 70% nitrogen and 30% argon. The predicted maximum velocities under the total gas flow rate of 8.5 SLPM and 10 SLPM are similar with other arc plasma torches.

About 90% of the cross-sectional area is at a temperature of over 15 000 K, and the temperature is strongly peaked in the center. The temperature distributions under the three different gas flow rates are separately shown in figure 14(f). These results in figure 14(e) are all higher than other arc plasma torches.

Our results suggest that generation of a long and stable plasma jet downstream of the nozzle exit should not only focus on a relatively low gas flow rate, but depends instead on a combination of factors, including the arc length, the properties of the gases, the power supply, and the aerodynamic characteristics of the channel flow, particularly in the anode region and downstream of the anode. All these factors are important to the formation and maintenance of a long plasma jet.

5. Summary and conclusions

A 3D magneto-hydrodynamics and RNG-turbulence transport modelling approach is applied to study the flow from a novel plasma spray torch operating with a mixture of 70% nitrogen and 30% argon at the constant current of 160 A and three different gas flow rates of 8.5 SLPM, 10 SLPM and 14 SLPM. The narrow circular gap between the cathode rod and the channel wall at the gas inlet can generate large pressure gradients and accelerate the flow in the downstream direction. Moreover, the unique trumpet-liked shape of the anode can induce separation of the channel flow and expand the arc column, reducing the compression effect of the cold boundary layer on the thermal arc column.

The maximum velocities at the nozzle exit when operate at the current of 160 A by using 70% nitrogen and 30% argon in volume are predicted to be 1474.5 m s^{-1}, 1506.8 m s^{-1} and 2024 m s^{-1} under the total gas flow rates of 8.5 SLPM, 10 SLPM and 14 SLPM, respectively. Moreover, the length of plasma jet at the same experimental conditions is decreased by the increasing of total gas flow rates. The maximum temperature at the nozzle exit under these three different conditions is in the range of 16 979 K to 17 173 K. The flow at the nozzle exit had higher temperature compared to other direct current non-transferred arc plasma torches.

Acknowledgments

The authors are grateful to Professor Ren-Zhong Huang from the Department of New Materials of Guangzhou Non-Ferrous Metal Research Institute for selfless help with computer programming. This work was supported by the Natural Key R&D Program of China (Basic Research Project, Grant No. 2017YFB0306104) and National Natural Science Foundation of China (Grant No. 91860114), the PhD Short-term Academic Visiting Program of Graduate School of Xi'an Jiaotong University and National PhD Degree Program of the China Scholarship Council. The authors are grateful to Massachusetts Green High-Performance Computing Center (MGH- PCC).

ORCID iDs

Sen-Hui Liu https://orcid.org/0000-0002-8979-5772
Juan Pablo Trelles https://orcid.org/0000-0002-7164-6509
Anthony B Murphy https://orcid.org/0000-0002-2820-2304

References

[1] Zhukov M F 2006 Electric arc generators of thermal plasma (review) *Plasma Devices Oper.* **5** 1–36
[2] Rat V, Mavier F and Coudert J F 2017 Electric arc fluctuations in DC plasma spray torch *Plasma Chem. Plasma Process.* **37** 549–80
[3] Nogues E, Vardelle M, Fauchais P and Granger P 2008 Arc voltage fluctuations: comparison between two plasma torch types *Surf. Coat. Technol.* **202** 4387–93

[4] Fauchais P L, Heberlein J V R and Boulos M I 2014 *Thermal Spray Fundamentals* (Berlin: Springer)

[5] Kuz'Min V I, Solonenko O P and Zhukov M F 1995 Application of DC plasma torch with a quasi-laminar jet outflow *1995 National Thermal Spray Conf. (Houston, TX, United States)* p11–5

[6] Liu S-H, Li C-X, Li L, Huang J-H, Xu P, Hua Y-Z, Yang G-J and Li C-J 2018 Development of long laminar plasma jet on thermal spraying process: microstructures of zirconia coatings *Surf. Coat. Technol.* **337** 241–9

[7] He-Ping L and Xi C 2002 Three-dimensional modelling of the flow and heat transfer in a laminar non-transferred arc plasma torch *Chin. Phys.* **11** 44–9

[8] Cheng K, Chen X and Pan W 2006 Comparison of laminar and turbulent thermal plasma jet characteristics—a modeling study *Plasma Chem. Plasma Process.* **26** 211–35

[9] Xu D-Y, Kai C, Xi C and Pan W X 2006 Modeling of a laminar DC arc plasma torch *Xi'an: Int. Conf. on Gas Discharge and Their Applications* (*11 September)*

[10] Xu D-Y, Chen X and Cheng K 2003 Three-dimensional modelling of the characteristics of long laminar plasma jets with lateral injection of carrier gas and particulate matter *J. Phys. D: Appl. Phys.* **36** 1583–94

[11] Yi P 2012 Numerical simulation study on flow fields in a non-transferred direct current plasma generator operating at reduced pressure *MD Thesis* Institute of Mechanics, China Academy of Science

[12] Wang H X, Xi C and Pan W X 2007 Comparison of the characteristics of laminar and turbulent impinging plasma jets *J. Eng. Thermophys.* **28** 7–9

[13] Pan W X, Xian M, Li T, Xi C and Wu C K 2008 Experimental observation on the stability and the 3D charactreisics of laminar/turbulent plasma jets *J. Eng. Thermophys.* **29** 2–4

[14] Xian M, Pan W X and Wu C K 2004 Temperarture and velocity measurement of laminar plasma jet *J. Eng. Thermophys.* **24** 5–7

[15] Xian M, Pan W X and Wu C K 2005 Transient measurement and analysis on heat flux distribution of partially ionized high temperature laminar flow jet *J. Eng. Thermophys.* **26** 137–9

[16] Gleizes A, Gonzalez J J and Freton P 2005 Thermal plasma modelling *J. Phys. D: Appl. Phys.* **38** R153–83

[17] Blais A, Proulx P and Boulos M 2003 Three-dimensional numerical modelling of a magnetically deflected dc transferred arc in argon *J. Phys. D: Appl. Phys.* **36** 488–96

[18] Moreau E, Chazelas C, Mariaux G and Vardelle A 2006 Modeling the restrike mode operation of a DC plasma spray torch *J. Therm. Spray Technol.* **15** 524–30

[19] Selvan B and Ramachandran K 2009 Comparisons between two different three-dimensional arc plasma torch simulations *J. Therm. Spray Technol.* **18** 846–57

[20] Freton P, Gonzalez J-J and Escalier G 2009 Prediction of the cathodic arc root behavior in a hollow cathode thermal plasma torch *J. Phys. D: Appl. Phys.* **42** 195–205

[21] Bernardi D, Colombo V, Ghedini E and Mentrelli A 2003 Comparison of different techniques for the FLUENT-based treatment of the electromagnetic field in inductively coupled plasma torches *Eur. Phys. J.* D **27** 55–72

[22] Scott D A, Kovitya P and Haddad G N 1989 Temperatures in the plume of a dc plasma torch *J. Appl. Phys.* **66** 5232–9

[23] Bauchire J M, Gonzalez J J and Gleizes A 1997 Modeling of a DC plasma torch in laminar and turbulent flow *Plasma Chem. Plasma Process.* **17** 409–32

[24] Li H-P, Pfender E and Chen X 2003 Application of Steenbeck's minimum principle for three-dimensional modelling of DC arc plasma torches *J. Phys. D: Appl. Phys.* **36** 1084–96

[25] Yuan X Q, Li H, Zhao T Z, Wang F, Guo W K and Xu P 2004 Comparative study of flow characteristics inside plasma torch with different nozzle configurations *Plasma Chem. Plasma Process.* **24** 585–601

[26] Ghorui S, Heberlein J V R and Pfender E 2007 Non-equilibrium modelling of an oxygen-plasma cutting torch *J. Phys. D: Appl. Phys.* **40** 1966–76

[27] Muggli F A, Molz R J, McCullough R and Hawley D 2007 Improvement of plasma gun performance using comprehensive fluid element modeling: part I *J. Therm. Spray Technol.* **16** 677–83

[28] Ye R, Proulx P and Boulos M I 1999 Turbulence phenomena in the radio frequency induction plasma torch *Int. J. Heat Mass Transfer* **42** 1585

[29] Zhou Q, Yin H, Li H, Xu X, Liu F, Guo S and Xu P 2009 Comparative study of turbulence models on highly constricted plasma cutting arc *J. Phys. D: Appl. Phys.* **42** 95208

[30] Huang R, Fukanuma H, Uesugi Y and Tanaka Y 2011 An improved local thermal equilibrium model of DC arc plasma torch *IEEE Trans. Plasma Sci.* **39** 1974–82

[31] Deng J, Li Y, Xu Y and Sheng H 2011 Numerical simulation of fluid flow and heat transfer in a DC non-transferred arc plasma torch operating under laminar and turbulent conditions *Plasma Sci. Technol.* **13** 201–7

[32] Huang R, Fukanuma H, Uesugi Y and Tanaka Y 2012 Simulation of arc root fluctuation in a DC non-transferred plasma torch with three-dimensional modeling *J. Therm. Spray Technol.* **21** 636–43

[33] Tsai J H, Hsu C M and Hsu C C 2013 Numerical simulation of downstream kinetics of an atmospheric pressure nitrogen plasma jet using laminar, modified laminar, and turbulent models *Plasma Chem. Plasma Process.* **33** 1121–35

[34] Guo Z, Yin S, Liao H and Gu S 2015 Three-dimensional simulation of an argon—hydrogen DC non-transferred arc plasma torch *Int. J. Heat Mass Transfer* **80** 644–52

[35] Murphy A B, Boulos M I, Colombo V, Fauchais P, Ghedini E, Gleizes A, Mostaghimi J, Proulx P and Schram D C 2008 Advanced thermal plasma modelling *High Temp. Mater. Process.* **12** 255–336

[36] El-Hadj A A and Ait-Messaoudene N 2005 Comparison between two turbulence models and analysis of the effect of the substrate movement on the flow field of a plasma jet *Plasma Chem. Plasma Process.* **25** 699–722

[37] Yakhot V and Orszag S A 1986 Renormalization group analysis of turbulence. I. Basic theory *J. Sci. Comput.* **1** 3

[38] ANSYS FLUENT 16.0 User's Guide (https://studentcommunity.ansys.com/thread/fluent-theory-guide-user-guide/)

[39] Colombo V and Ghedini E 2005 Time dependent 3-D simulation of a DC non-transferred arc plasma torch: anode attachment and downstream region effects *Proc. 17th Int. Symp. on Plasma Chemistry (Toronto, Canada)*

[40] Trelles J P, Chazelas C, Vardelle A and Heberlein J V R 2009 Arc plasma torch modeling *J. Therm. Spray Technol.* **18** 728–52

[41] Lowke J J 1974 Predictions of arc temperature profiles using approximate emission coefficients for radiation losses *J. Quant. Spectrosc. Radiat. Transfer* **14** 111–22

[42] Gleizes A, Cressault Y and Teulet P 2010 Mixing rules for thermal plasma properties in mixtures of argon, air and metallic vapours *Plasma Sources Sci. Technol.* **19** 55013

[43] Boulos M, Fauchais P and Pfender E 1994 *Thermal Plasmas: Fundamentals and Applications* (Berlin: Springer)

[44] Xi C 2009 *Heat and Mass Transfer of Thermal Plasma* (Beijing: Science Press) pp 534–47

[45] Pateyron B, Elchinger M-F, Delluc G and Fauchais P 1992 Thermodynamic and transport properties of Ar–H_2 and Ar–He plasma gases used for spraying at atmospheric pressure. I: properties of the mixtures *Plasma Chem. Plasma Process.* **12** 421–48

[46] Murphy A B 1996 A comparison of treatments of diffusion in thermal plasmas *J. Phys.* D **29** 1922–32
[47] Murphy A B 1993 Diffusion in equilibrium mixtures of ionized gases *Phys. Rev.* E **48** 344
[48] Murphy A B and Arundelli C J 1994 Transport coefficients of argon, nitrogen, oxygen, argon-nitrogen, and argon-oxygen plasmas *Plasma Chem. Plasma Process.* **14** 451–90
[49] Murphy A B 2001 Thermal plasmas in gas mixtures *J. Phys. D: Appl. Phys.* **34** R151–73
[50] Liu S-H, Zhang S-L, Li C-X, Li L, Huang J-H, Trelles J P, Murphy A B and Li C-J 2019 Generation of long laminar plasma jets: experimental and numerical analyses *Plasma Chem. Plasma Process.* **39** 1–18
[51] Liu S H, Zhang H Y, Wang Y P, Ji G, Li L, Xu P, Huang J-H, Zhang S-L, Li C-X and Li C J 2019 Microstructural evolution of alumina coatings by a novel long laminar plasma spraying method *Surf. Coat. Technol.* **363** 210–20
[52] Liu S H, Li C X, Zhang H Y, Zhang S L, Li L, Xu P, Yang G-J and Li C J 2018 A novel structure of YSZ coatings by atmospheric laminar plasma spraying technology *Scr. Mater.* **153** 73–6
[53] Choudhury D 1993 *Introduction to the Renormalization Group Method and Turbulence Modeling* (Fluent Inc.) Technical Memorandum TM-107 USA
[54] Yakhot V and Orszag S A 1986 Renormalization group analysis of turbulence: I. Basic theory *J. Sci. Comput.* **1** 51
[55] ANSYS FLUENT 12.0 UDF Manual (https://studentcommunity.ansys.com/thread/fluent-theory-guide-user-guide/)
[56] Hsu K C, Etemadi K and Pfender E 1983 Study of the free-burning high-intensity argon arc *J. Appl. Phys.* **54** 1293–301
[57] Trelles J P, Pfender E and Heberlein J V R 2007 Modelling of the arc reattachment process in plasma torches *J. Phys. D: Appl. Phys.* **40** 5635–48
[58] Murphy A B 2012 Transport coefficients of plasmas in mixtures of nitrogen and hydrogen *Chem. Phys.* **398** 64–72
[59] Cram L E 1985 Statistical evaluation of radiative power losses from thermal plasmas due to spectral lines *J. Phys. D: Appl. Phys.* **18** 401–11
[60] Ernst K A, Kopainsky J G and Maecker H H 1973 The energy transport, including emission and absorption, in N_2-arcs of diffusion rad II *IEEE Trans. Plasma Sci.* **1** 3–16
[61] Murphy A B 2009 Modelling of thermal plasmas for arc welding: the role of the shielding gas properties and of metal vapor *J. Phys. D: Appl. Phys.* **42** 1–20
[62] Duan Z and Heberlein J 2002 Arc instabilities in a plasma spray torch *J. Therm. Spray Technol.* **11** 44–51
[63] Trelles J P, Heberlein J V R and Pfender E 2007 Non-equilibrium modelling of arc plasma torches *J. Phys. D: Appl. Phys.* **40** 5937–52
[64] Fauchais P, Vardelle A and Dussoubs B 2001 *Quo vadis* thermal spraying? *J. Therm. Spray Technol.* **10** 44–66
[65] Fauchais P 2004 Understanding plasma spraying *J. Phys. D: Appl. Phys.* **37** R86–108